

# Atomic altermagnetism

Rodrigo Jaeschke-Ubiergo,<sup>1</sup> Venkata-Krishna Bharadwaj,<sup>1</sup> Warley Campos,<sup>2</sup> Ricardo Zarzuela,<sup>1</sup> Nikolaos Biniskos,<sup>3</sup> Rafael M. Fernandes,<sup>4,5</sup> Tomas Jungwirth,<sup>6,7</sup> Jairo Sinova,<sup>1</sup> and Libor Šmejkal<sup>2,8,1,6</sup>

<sup>1</sup>*Institut für Physik, Johannes Gutenberg Universität Mainz, D-55099 Mainz, Germany*

<sup>2</sup>*Max Planck Institute for the Physics of Complex Systems, Nöthnitzer Str. 38, 01187 Dresden, Germany*

<sup>3</sup>*Charles University, Faculty of Mathematics and Physics, Department of Condensed Matter Physics, Ke Karlovu 5, 121 16, Praha, Czech Republic*

<sup>4</sup>*Department of Physics, The Grainger College of Engineering, University of Illinois Urbana-Champaign, Urbana, IL 61801, USA*

<sup>5</sup>*Anthony J. Leggett Institute for Condensed Matter Theory, The Grainger College of Engineering, University of Illinois Urbana-Champaign, Urbana, IL 61801, USA*

<sup>6</sup>*Institute of Physics, Czech Academy of Sciences, Cukrovarnická 10, 162 00, Praha 6, Czech Republic*

<sup>7</sup>*School of Physics and Astronomy, University of Nottingham, NG7 2RD, Nottingham, United Kingdom*

<sup>8</sup>*Max Planck Institute for Chemical Physics of Solids, Nöthnitzer Str. 40, 01187 Dresden, Germany*  
(Dated: March 17, 2025)

Altermagnetism has been recently experimentally verified by photoemission mapping of the spin order in momentum space in MnTe and CrSb, which feature two anisotropic sublattices with antiparallel magnetic dipole moments. In this work, we explicitly demonstrate the presence of an even-parity ferroically ordered non-dipolar spin density on atomic sites, i.e. atomic altermagnetism, in MnTe, La<sub>2</sub>O<sub>3</sub>Mn<sub>2</sub>Se<sub>2</sub> and Ba<sub>2</sub>CaOsO<sub>6</sub>. We do so through spin-symmetry analysis and partial-wave decomposition of the spin density obtained by first-principles calculations. In MnTe we show a ferroically ordered *g*-wave form factor in the spin density around the Mn site. In the A<sub>2</sub>O<sub>3</sub>M<sub>2</sub>Se<sub>2</sub> family (A= La, Sr and M= Mn, Fe, Co), we show that there is a ferroically ordered *d*-wave form factor coexisting with the antiferroic magnetic dipoles in the M site, while the O site shows no dipole but a pure *d*-wave atomic spin density. In the Mott-insulating Ba<sub>2</sub>CaOsO<sub>6</sub>, as a key result, we reveal a pure form of atomic altermagnetism – absent of any dipolar sublattice order. This highlights that the altermagnetic order can exist without a Néel vector formed by antiferroic dipole moments on an even number of crystal sublattices, underlining its distinction from collinear Néel antiferromagnetic order. Our calculations predict that La<sub>2</sub>O<sub>3</sub>Mn<sub>2</sub>Se<sub>2</sub> and Ba<sub>2</sub>CaOsO<sub>6</sub> can exhibit giant spin-splitter angles of up to 42° and 26° respectively, thus demonstrating the possibility of large altermagnetic responses without requiring the staggered Néel order of local dipole moments.

Altermagnetism is a recently identified new type of magnetism characterized by spin order in both direct and momentum space with *d*-, *g*-, or *i*-wave symmetry [1]. Altermagnetism was predicted by a rigorous classification and delimitation of collinear magnetic phases based on spin symmetries that involve pairs of generally distinct operations, acting on the lattice and spin degrees of freedom [1]. These spin symmetries lead to an unconventional complex altermagnetic spin density [2] and exchange fields [3], which break the underlying lattice symmetry in an analogous way to what occurs in unconventional superfluid states [4, 5]. Recently, altermagnetism has been experimentally confirmed by momentum-space and direct-space photoemission spectroscopy and microscopy in representative binary-compounds MnTe and CrSb with ordering above room temperature [6–15].

The discovery of the altermagnetic spin symmetry class also provided a unifying explanation of the previous reports of unconventional time-reversal symmetry breaking (TRSB) in the electronic structure and related effects, such as the anomalous Hall effect [2, 16], spin currents [17–20] and magneto-optical effects [16, 21]. The unconventional electronic structure of altermagnets exhibits TRSB spin-split bands across the entire Brillouin

Zone, except along 2 (*d*-wave), 4 (*g*-wave) or 6 (*i*-wave) nodal surfaces [2, 16], leading to various spintronic effects [2, 16, 18, 20, 22–25].

The theoretically predicted and experimentally confirmed altermagnets are hitherto characterized by an even number of magnetic sublattices, whose alternating magnetic moments are accompanied by an alternating orientation of the atomic site environment in direct space [1, 4, 24, 26]. In a typical *d*-wave altermagnet, the alternating magnetic sublattices are related by a 180° spin rotation combined with a lattice rotation (proper or improper). This alternation of magnetic sites is commonly achieved by the anisotropic crystal environment of the magnetic sublattices [1, 2], but can also be achieved by electronic correlations [27, 28].

In this letter we address the ferroic nature of altermagnets, by studying the partial-wave expansion of their direct-space spin density. Previous reports have shown that some altermagnetic candidates host ferroically ordered magnetic multipoles on the magnetic sublattices [29–31]. Both approaches aim to describe the anisotropy of the spin density beyond the dipolar approximation (*s*-wave), and, while being complementary, they are also fundamentally distinct. The magnetic multipoles approach is inspired in classical

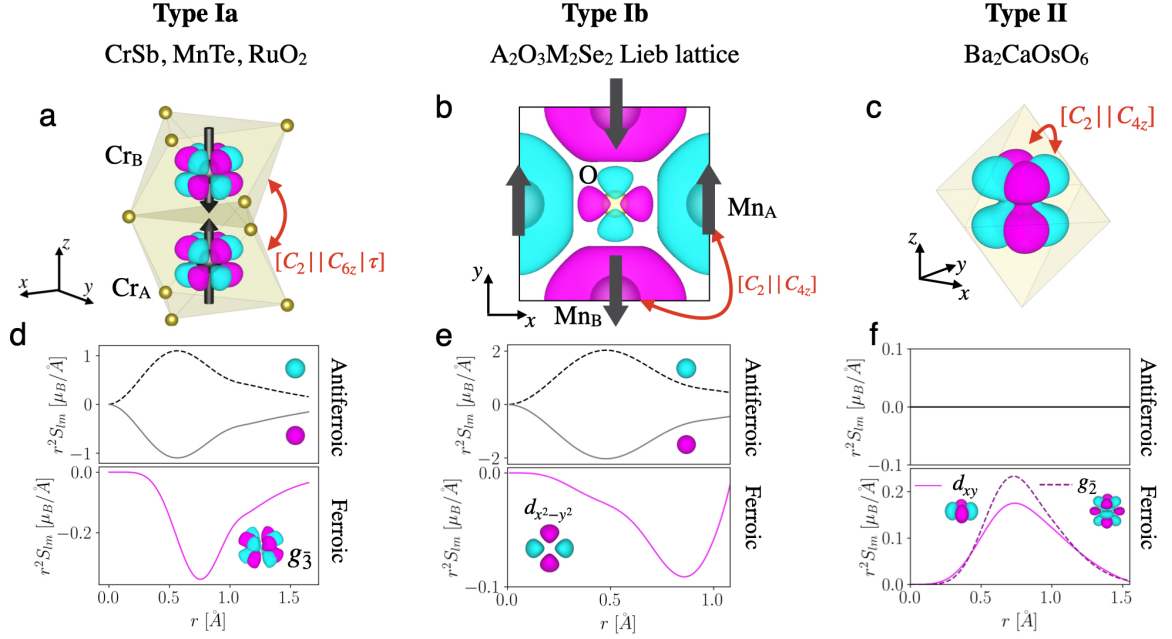


FIG. 1. Partial-wave expansion of the spin density from non-relativistic DFT calculations on CrSb,  $A_2O_3M_2Se_2$ , and  $Ba_2CaOsO_6$ . (d), (e) and (f) show the radial dependence of the relevant partial-wave components  $S_{lm}(r)$  as defined in the main text. (a) CrSb unit cell, where black arrows represent the magnetic dipoles and, superimposed, we show the ferrially ordered  $g_3 = Y_{4,-3}$  harmonic. (d) Radial dependence of the order parameters. (top) Antiferroic  $s$ -wave on each sublattice, (bottom) ferroic  $g$ -wave form factor. (b) Unit cell of  $La_2O_3Mn_2Se_2$  with an iso-surface of the spin density. Mn sites have opposite magnetic dipole moments, and O site has no dipole but a  $d_{x^2-y^2}$  spin density. (e) (top)  $s$ -wave harmonic expansion centered at each Mn site. (bottom)  $d$ -wave direct-space order parameter, formed by adding up the  $d_{x^2-y^2}$  contributions of  $Mn_A$ ,  $Mn_B$  and O sublattices. (c) Total spin density iso-surface around the Os site in  $Ba_2CaOsO_6$  within its octahedral environment. (f) shows the respective relevant partial-waves, with zero  $s$ -wave contribution (no magnetic dipole) and two ferroic  $d$ -wave harmonics  $d_{xy}$  and  $g_2 \equiv Y_{4,-2}$ .

electromagnetism, while the partial-waves analysis arises from atomic physics. We show that the use of partial waves reveals a direct correlation between the anisotropy of the atomic spin density in direct-space, and the spin-splitting of the electronic band structure in momentum space.

Here we demonstrate the presence of a ferrially ordered  $g$ -wave form factor of the atomic spin density in CrSb and MnTe, which we consider here to be canonical altermagnets. We show that the ferrially ordered  $g$ -wave spin density coexists with an antiferroic (antiparallel) order of the atomic magnetic dipole moments (Néel order). In  $A_2O_3M_2Se_2$  ( $A = La, Sr$  and  $M = Mn, Fe, Co$ ) with a Lieb lattice structure formed by the M and O sites, we demonstrate a mixture of, in the one hand, a ferrially ordered  $d$ -wave spin density with antiferroic magnetic dipoles at the M sites, and in the other hand a pure  $d$ -wave atomic spin density (no magnetic dipole) around the O site.

As a key result, we further propose a pure form of atomic altermagnetism, i.e., a direct-space spin density without any dipolar moments at any atomic site but with an on-site ferrially ordered  $d$ -,  $g$ - or  $i$ -wave form factor, thus enabling the realization of altermagnetism without

the need to have the staggered Néel order of local dipole moments. In addition, we show that strong correlations can conspire with orbital states to generate an on-site altermagnetic  $d$ -wave spin density, without being promoted by the symmetry of the ionic-crystal lattice. We demonstrate such an atomic altermagnetic state both in the non-relativistic limit and in the presence of the relativistic spin-orbit coupling (SOC) in the  $Ba_2CaOsO_6$  material [32–34].

It is well established that  $d$ -wave altermagnets can host spin-dependent conductivities, leading to giant-magnetoresistance (GMR) [20] and spin-splitter effects [18, 19, 35]. In the latter case, a pure spin current flows transverse to the applied electric bias. We calculate a large spin-splitter response in both  $A_2O_3M_2Se_2$  and  $Ba_2CaOsO_6$ , demonstrating that the altermagnetic spin density on a single atomic site without Néel order, i.e., a pure atomic altermagnet (in the case of  $Ba_2CaOsO_6$ ), can generate spin-splitter effect.

*Partial-wave expansion of the spin density* – The spin density, as a property of the Fermi sea, can be defined as  $\mathbf{S}(\mathbf{r}) = \frac{\hbar}{2} \sum_{\mathbf{k}, n} f_{n\mathbf{k}} \psi_{n\mathbf{k}}^\dagger(\mathbf{r}) \boldsymbol{\sigma} \psi_{n\mathbf{k}}(\mathbf{r})$ , where  $\psi_{n\mathbf{k}}(\mathbf{r})$  is the spinorial eigenfunction of wave-vector  $\mathbf{k}$  and band index  $n$ ,  $f_{n\mathbf{k}}$  is the occupation number and

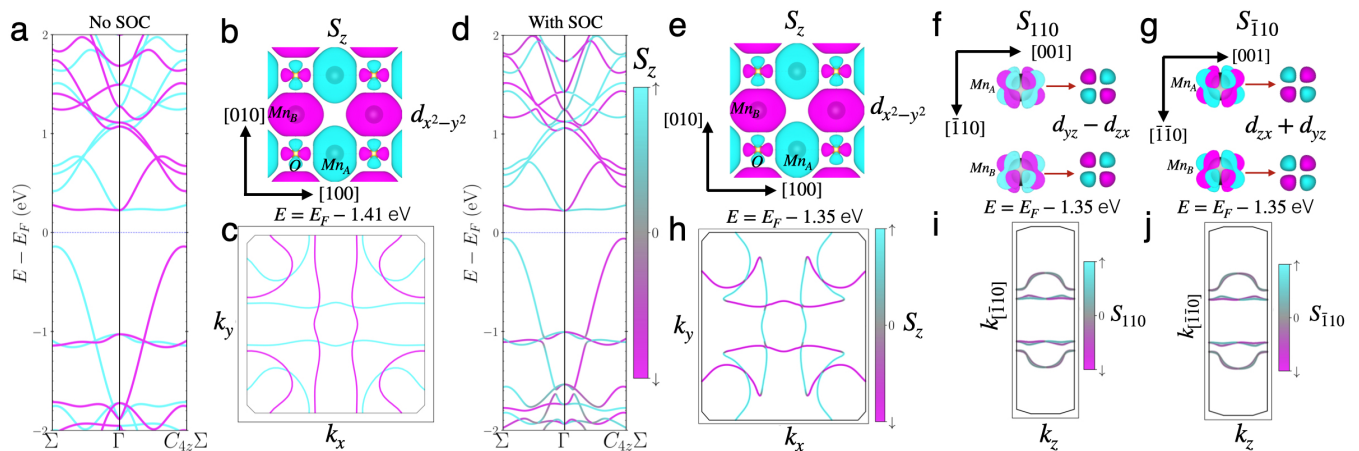


FIG. 2. DFT calculation for  $\text{La}_2\text{O}_3\text{Mn}_2\text{Se}_2$ , without (a-c) and with (d-j) SOC. (a) and (d) Band structure with  $S_z$  spin polarization showed in color-scale. (b) Iso-surface of the non-relativistic spin density. (c) Energy iso-surface cut in the plane  $k_z = 0$ . (e-g) Iso-surface of the spin density (with SOC) from different views, projected along the spin components  $[001]$  (e),  $[110]$  (f) and  $[\bar{1}\bar{1}0]$  (g). Next to each spin component we highlight the ferroically ordered partial-wave of the spin density:  $d_{x^2-y^2}$  (e),  $d_{zx} - d_{yz}$  (f) and  $d_{zx} + d_{yz}$  (g). Iso-energy lines on planes that contain the  $\Gamma$  point and are normal to the directions  $[001]$  (h),  $[110]$  (i) and  $[\bar{1}\bar{1}0]$  (j), with the color scale representing the spin polarization on the axis normal to the planes.

$\sigma$  are the Pauli matrices representing the spin degree of freedom. We define  $\mathbf{S}_\alpha(\mathbf{r}) = \mathbf{S}(\mathbf{r} - \mathbf{r}_\alpha)$  as the spin density with respect to an atomic site  $\mathbf{r}_\alpha$ , and we further expand each spin component in spherical harmonics as  $S_\alpha^i(\mathbf{r}) = \sum_{lm} S_{\alpha,lm}^i(r) Y_{lm}(\theta, \phi)$  where  $Y_{lm}(\theta, \phi)$  are real spherical harmonics [36] and  $(r, \theta, \phi)$  denote the spherical coordinates of  $\mathbf{r} - \mathbf{r}_\alpha$ . The magnetic dipole approximation allows us to define an on-site magnetic dipole as the radial integral of the first term in the expansion  $S_{\alpha,00}^i(r)$ . The magnetic dipoles alone, however, are unable to capture the ferroic nature of altermagnetism [29, 30].

*Canonical altermagnets* – In a canonical altermagnet, such as CrSb (Type Ia in Fig. 1a,d), the magnetic dipoles align antiferroically, but the spin density around each magnetic site is anisotropic. For CrSb there is a ferroically ordered contribution with the symmetries of a  $g_{\bar{3}} \equiv Y_{4,-3}$  harmonic (See Fig. 1d). Remarkably, unlike conventional multipolar orders which originate from SOC [37, 38], the ferroic order in the above altermagnets is stabilized by the antiferroic magnetic dipoles distributed in the crystal according to the altermagnetic spin group symmetry [1]. The  $g_{\bar{3}}$  harmonic has the same nodal structure as the spin splitting in the electronic band structure, which results from the spin group of CrSb containing operations such as  $[C_2||C_{6z}|\bar{\tau}]$  combining a two-fold spin rotation with a six-fold lattice rotation, and a half unit cell translation along the z-axis as marked in Fig. 1a. In the Supplementary Information (SI), we show similar analysis for MnTe.

*Lieb lattice candidate* – Next we discuss the  $\text{A}_2\text{O}_3\text{M}_2\text{Se}_2$  family (with special focus on  $\text{A}=\text{La}$ ,  $\text{M}=\text{Mn}$ ). The crystal structure is body centered tetragonal with space group  $I4/mmm$  (No. 139) [39–41]. The Mn atoms are located at the Wyckoff position 4c,

and together with the oxygen ligands located at Wyckoff position 2b, they form a layered structure that resembles the Lieb lattice [42, 43].

The total spin density obtained by density-functional theory (DFT), without spin-orbit coupling, is shown in Fig. 1b. While  $\text{La}_2\text{O}_3\text{Mn}_2\text{Se}_2$  is a Mott insulator, the symmetries of the spin density in both direct and momentum space can be captured by DFT. We decompose this spin density into spherical harmonics around Mn and O sites. In the Mn site, besides the  $s$ -wave staggered magnetic dipoles (see top panel in Fig 1e) we identify two ferroically ordered contributions with the symmetries of the  $d_{x^2-y^2}$  and  $g_2 \equiv Y_{4,2}$  harmonics. Both partial waves have the same  $d$ -wave nodal structure, and they deform the otherwise spherically symmetric spin density. In the Oxygen site, which has no magnetic dipole moment, we see that its atomic spin density is fully described by a  $d_{x^2-y^2}$  form factor. In the bottom panel of Fig. 1e we show the  $d$ -wave direct-space order parameter that is obtained by adding up the  $d_{x^2-y^2}$  form factors on  $\text{Mn}_A$ ,  $\text{Mn}_B$  and O sublattices. Indeed, the spin density in the material follows the spin point group  $^2_4/m^1m^2m$ , which classifies it as a  $d$ -wave altermagnet. The electronic band structure is spin-split (see Fig. 2a), with spin splitting reaching a 1 eV scale, and the spin polarization of the energy iso-surfaces in momentum space (Fig. 2c) shows the same  $d$ -wave character as the ferroically ordered  $d_{x^2-y^2}$  projection of the spin density in direct space (Fig. 2b).

A key factor behind the large splitting in the  $\text{A}_2\text{O}_3\text{M}_2\text{Se}_2$  family is the Lieb lattice structure. Here, the anisotropy of the exchange enters at the second Mn-Mn neighbor. If we consider the  $\text{Mn}_A$  sublattice, the links with neighbors at  $(a, 0, 0)$  and  $(0, a, 0)$  are different,

because the first one contains the O-site in the middle. This anisotropic exchange at close distance can lead to large spin splitting and strength of the altermagnetic order.

We emphasize that, in the non-relativistic collinear regime, both the direct-space spin density and the momentum-space spin polarization of the band structure have spin degenerate nodal planes orthogonal to the directions  $[110]$  and  $[\bar{1}10]$ . When SOC is included in the DFT calculations (Néel order along  $[001]$ ), the nodal planes show a weak  $d$ -wave spin-splitting, with spin polarization normal to the respective plane. Thus, when looking at the plane in momentum space normal to the  $[110]$  axis that crosses the  $\Gamma$  point (Fig. 2i), the component  $S_{110}$  shows a  $d$ -wave character, with nodal planes normal to the  $[\bar{1}10]$  and  $[001]$  axes. The corresponding  $S_{110}$  component of the direct-space spin density displays the same  $d$ -wave nodal structure (Fig. 2f). Analogously, if we focus on the plane normal to the  $[\bar{1}10]$  axis, both the direct-space spin density (Fig. 2g), and the spin polarization of the energy iso-surface (Fig. 2j) have nodal planes normal to the  $[110]$  and  $[001]$  axes. Thus, there is a clear correspondence between the nodal structure of the direct-space spin density, and the spin polarization of the band structure in momentum space. More broadly, as we show below, each spin component displays a different  $d$ -wave form-factor, consistent with the analysis of Ref. [30]. A full characterization of the partial-wave decomposition of the direct space spin density for  $\text{La}_2\text{O}_3\text{Mn}_2\text{Se}_2$  can be seen in the SI.

In  $\text{La}_2\text{O}_3\text{Mn}_2\text{Se}_2$ , the  $[110]$  ( $[\bar{1}10]$ ) component of the spin density is two orders of magnitude smaller than the  $S_{001}$  component. Additional insight into the spin ordering in the presence of SOC is provided by the following minimal model:

$$h(\mathbf{k}) = \lambda_1(k_x^2 - k_y^2)\sigma_z + \lambda_2(k_y - k_x)k_z\sigma_{[110]} + \lambda_2(k_x + k_y)k_z\sigma_{[\bar{1}10]}, \quad (1)$$

where  $\mathbf{k}$  is the wave-vector and  $\sigma_z$ ,  $\sigma_{[110]}$ , and  $\sigma_{[\bar{1}10]}$  are defined as  $\boldsymbol{\sigma} \cdot \mathbf{v}$ , with  $\mathbf{v}$  a unit vector along  $[001]$ ,  $[110]$  and  $[\bar{1}10]$  respectively. Without SOC,  $\lambda_2 = 0$ , and when SOC is included the additional  $d$ -wave splitting is captured by  $\lambda_2$ , with  $\lambda_2 \ll \lambda_1$ . An important consequence of the existence of two nodal planes for each of the three independent spin directions is that the band structure will only be spin-degenerate along nodal lines in the presence of SOC rather than nodal planes.

*Pure atomic altermagnet candidate* – We consider now  $\text{Ba}_2\text{CaOsO}_6$ , whose crystal structure is face-centered cubic with space group  $Fm\bar{3}m$  (No. 225) [44]. The Os atom occupies the Wyckoff position  $4a$ . This material has drawn significant attention owing to unexpected oscillations in the zero-field muon spin relaxation [44],

which suggest a phase transition with TRSB at  $T \sim 50$  K. Based on neutron spectroscopy and  $X$ -ray diffraction measurements, it was proposed that this phase transition can be explained by a ferro-octupolar phase [32], with magnetic octupoles ordered on the Os  $5d^2$  electrons. Later on, this claim was supported from an *ab initio* perspective [45], using VASP and on-site density matrix control [46]. To our knowledge, however, little has been said about the connection between this ferro-octupolar phase and the spin splitting in the electronic band structure.

Despite SOC being strong in this double perovskite, it is still instructive to explore its non-relativistic limit, because also in this limit we find a correspondence between the direct and momentum space order parameters. We calculate the spin density from DFT, including correlations on the Os site using the Liechtenstein's spherically symmetric DFT+U approach [47], with parameters  $U = 3.2$  eV and  $J = 0.5$  eV, in agreement with the pioneer study on the compound [45]. Without SOC, the collinear spin density around the Os site is shown in Fig. 1c. Below, in Fig. 1f we see that the harmonic decomposition is given by  $d_{xy}$  and  $g_2 \equiv Y_{4,-2}$ . Both spherical harmonics have  $d$ -wave symmetry in the  $xy$  plane, but unlike  $\text{La}_2\text{O}_3\text{Mn}_2\text{Se}_2$ , the nodal planes are normal to  $[100]$  and  $[010]$ . There is no magnetic dipole moment, as can be seen in the top panel of Fig. 1f, making this material a pure atomic altermagnet. The corresponding iso-energy surfaces (Fig. 3c) follow the  $[C_2||C_{4z}]$  spin symmetry.

In Fig. 3a we show the band structure along a path in the  $(k_x, k_y)$ -plane that bisects the two nodal planes. We identify a spin splitting of 0.2 eV just below the Fermi level. We emphasize that, because  $\text{Ba}_2\text{CaOsO}_6$  is a Mott insulator, the bands crossing the Fermi level in Fig. 3a will be pushed away by the on-site repulsion. Further investigation of the impact of strong correlations on the band structure is, however, beyond the scope of our work, which focuses on the symmetry-enforced shape of the spin density on the Os site. In this regard, we note that the  $d_{xy}$  form factor of the spin density obtained via DFT+U is consistent with the strong-coupling perspective on the octupolar moment of Os  $5d^2$ , which can be understood as the  $z$ -component of the pseudo-spin that characterizes the non-Krammers doublet ground-state of the Os atom, arising from the combined effects of crystal fields and SOC on the localized  $J = 2$  state [33, 34].

Once SOC is included, the spin density in  $\text{Ba}_2\text{CaOsO}_6$ , in agreement with previous reports [45], becomes strongly noncoplanar, with equivalent  $d$ -wave form factors along the  $x$ ,  $y$ , and  $z$  axes. These results are consistent with the analysis of Ref. [30], which found that the inclusion of SOC makes the spin-density noncoplanar in some altermagnets. Figure 3d shows the band structure (with SOC) along a path in the  $x - y$  plane, bisecting the planes normal to  $[100]$  and  $[010]$  axes. We also show

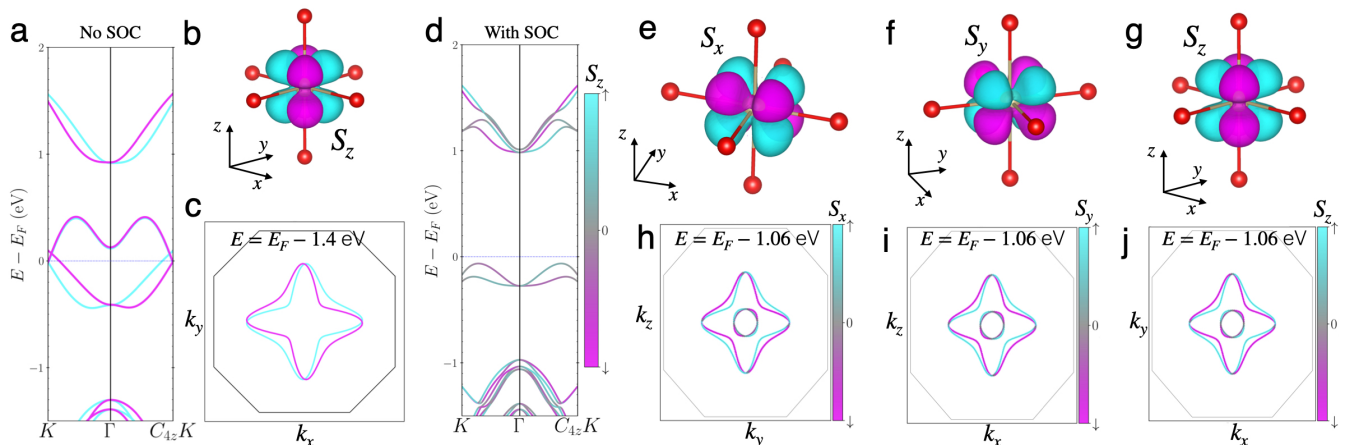


FIG. 3. DFT+U calculation for  $\text{Ba}_2\text{CaOsO}_6$  without (a-c) and with (d-j) SOC. (a), (d) Band structure colored according to the  $S_z$  spin polarization. (b) Iso-surface of the direct-space spin density (no SOC) around the Os site. (c) Energy iso-surface cut in the plane  $k_z = 0$ . Iso-surface of the spin density around the Osmium site (with SOC), projected along the spin components [100] (e), [010] (f) and [001] (g). Energy iso-surface cuts in planes that contain the  $\Gamma$  point and are normal to directions [100] (h), [010] (i) and [001] (j), with color scale representing the spin polarization along the axis normal to the planes.

the  $z$ -component of the spin polarization in a color scale. Note that, in the presence of SOC, the system displays a band gap of around 1 eV. We note, however, that strong correlations will render the material a Mott insulator.

The  $x$ ,  $y$  and  $z$  components of the spin density around the Os atom are shown in Figs. 3 e-g. Below each spin density, in Figs. 3 h-j, we show energy iso-surface cuts with the spin polarization (component normal to each plane) plotted in color scale. The spin density can be understood as 3 orthogonal  $d$ -wave form factors corresponding to the  $x$ ,  $y$  and  $z$  spin components. The nodal structure of the spin density is reflected in the spin polarization of the energy iso-surfaces. In analogy with Eq. 1, a simple model capturing these noncoplanar altermagnetic  $d$ -wave form factors is given by [30]:

$$h(\mathbf{k}) = \lambda k_x k_y \sigma_z + \lambda k_z k_x \sigma_y + \lambda k_y k_z \sigma_x. \quad (2)$$

Note that, because of the cubic symmetry of the crystal structure, and in contrast to  $\text{La}_2\text{O}_3\text{Mn}_2\text{Se}_2$ , all spin components have the same prefactor  $\lambda$ .

The emergence of the atomic  $d$ -wave form factors in  $\text{Ba}_2\text{CaOsO}_6$ , with or without SOC, comes from an interplay between correlations and orbital ordering. The on-site occupation matrix of the  $d$  orbitals captures the  $d$ -wave character [45], which then gets imprinted in both the direct-space spin density and the spin splitting in the band structure.

*Spin currents* – We calculate the magnitude of the spin currents in the non-relativistic limit for both  $\text{La}_2\text{O}_3\text{Mn}_2\text{Se}_2$  and  $\text{Ba}_2\text{CaOsO}_6$ , by quantifying the spin-splitter angle  $\alpha$ , which measures the efficiency in the charge-to-spin conversion, and the GMR coefficient [20]. Our results are shown in Fig. 4, where the spin-splitter

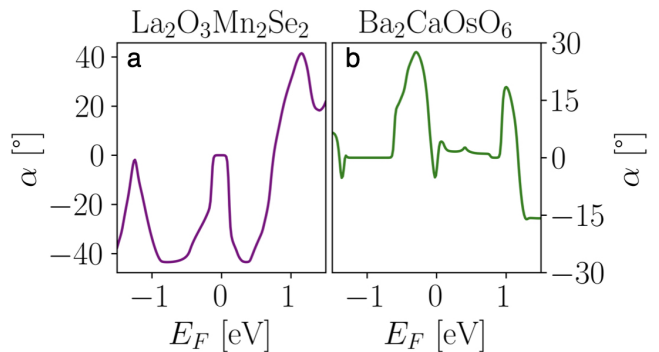


FIG. 4. Estimation of the spin-splitter angle for the non-relativistic calculation of both  $\text{La}_2\text{O}_3\text{Mn}_2\text{Se}_2$  (a) and  $\text{Ba}_2\text{CaOsO}_6$  (b). See in Supplementary Information the calculation of the GMR coefficients.

angle is plotted as a function of the Fermi energy. In the explored energy interval, the spin-splitter angle for  $\text{Ba}_2\text{CaOsO}_6$  (Fig. 4a) reaches a maximum of  $26^\circ$ , while for  $\text{La}_2\text{O}_3\text{Mn}_2\text{Se}_2$  it is even higher, reaching  $44^\circ$ . The GMR coefficient (see SI) in  $\text{La}_2\text{O}_3\text{Mn}_2\text{Se}_2$  reaches 900% for energies close to the Fermi energy, which is one order of magnitude higher than the 100% scale of the initial altermagnetic GMR prediction, considering  $\text{RuO}_2$  [20]. While  $\text{La}_2\text{O}_3\text{Mn}_2\text{Se}_2$  is not metallic, we expect the spin-splitter angle and the GMR coefficient to be equally large in related metallic altermagnetic candidates on layered Lieb lattices, such as  $\text{UCr}_2\text{Si}_2\text{C}$  [48],  $\text{KV}_2\text{Se}_2\text{O}$  [49] or  $\text{RbV}_2\text{Se}_2\text{O}$  [50]. In addition to the  $d$ -wave form factor in the sites hosting the magnetic dipoles, the  $d$ -wave atomic spin density will be present, without dipole, at the O site in  $\text{RbV}_2\text{Se}_2\text{O}$  and  $\text{KV}_2\text{Se}_2\text{O}$ , and at the U site at  $\text{UCr}_2\text{Si}_2\text{C}$ . In the SI, we show calculations of

the electronic structure for  $\text{UCr}_2\text{Si}_2\text{C}$ , and we comment as well on the nature of the spin conductivity tensor in  $\text{Ba}_2\text{CaOsO}_6$  (with SOC), when the spin density is described by three noncoplanar  $d$ -wave form factors.

*Discussion* – While the notion of multipolar magnetism is naturally connected with altermagnetism [29, 30], one should be careful when comparing these two concepts. Not every direct-space ferroically ordered magnetic multipole, corresponds to the collinear  $d$ -,  $g$ -, or  $i$ -wave altermagnetic order with the characteristic anisotropic nodal spin polarization in the momentum-space electronic structure. As an illustrative example, consider  $\text{Mn}_3\text{Sn}$ , which has a phase between  $T_{N2} = 50\text{K}$  and  $T_{N1} = 420\text{K}$  in which Mn magnetic moments form an inverse triangular spin structure. Although the material exhibits octupolar order  $T_x^\gamma$  [51], its magnetic order on the crystal is non-collinear and, therefore, is not altermagnetic. Correspondingly, the resulting spin polarization in the momentum space takes noncollinear and nodeless form [52].

*Conclusions*— In this work we extend the known mechanisms that induce altermagnetism, to include pure atomic altermagnetism. The interplay between strong correlations and orbital occupation (possibly with strong SOC) generates a spin density which lacks magnetic dipole moments, while having a  $d$ -wave component which is also reflected in the corresponding spin-polarization symmetry of the electronic structure in the momentum space. In  $\text{La}_2\text{O}_3\text{Mn}_2\text{Se}_2$  we demonstrate the coexistence of dipole and higher-order partial-wave components on the Mn-sites, with the absence of the dipole and the presence of the higher-order partial-wave component (atomic altermagnetism) on the O-sites. We estimate the spin-splitter angle and the GMR coefficient in this material as 44 degrees and 900%, respectively.

We identified pure atomic altermagnetism with  $d$ -wave symmetry in the non-relativistic limit of  $\text{Ba}_2\text{CaOsO}_6$ . When including SOC, the spin density has the structure of three noncoplanar (and orthogonal)  $d$ -waves form factors. In all cases, we identify one-to-one correspondence between the ferroically ordered  $d$ -wave harmonic of the spin density in direct space, and the angular dependence of the spin splitting around the  $\Gamma$  point.

This work thus extends the search for altermagnetic candidates to materials that, while breaking time-reversal symmetry, do not have dipolar order. The detection of the magnetic order without local magnetic dipoles might represent an intriguing challenge for the conventional techniques like neutron scattering. The spin-polarized electronic structure, and the spintronic responses associated with the altermagnetic order, can serve as experimental probes of these higher-order partial-wave forms of magnetic ordering. Besides  $\text{Ba}_2\text{CaOsO}_6$ , there is a range of materials that have been previously identified as candidates for magnetic

octupolar order that may deserve further investigation, in the context of the higher-partial-wave ordering and atomic altermagnetism [37, 53–56], including the metallic cage compound  $\text{PrV}_2\text{Al}_2\text{O}$ , which has recently drawn significant attention [57–61].

*Acknowledgments*— RJU, VKB, RZ, JS and LS acknowledge funding by the Deutsche Forschungsgemeinschaft (DFG, German Research Foundation)- TRR 173– 268565370 (project A03) and TRR 288– 422213477 (project A09 and B05). TJ acknowledges Ministry of Education of the Czech Republic Grant CZ.02.01.01/00/22008/0004594 and ERC Advanced Grant no. 101095925. R.M.F. was supported by the Air Force Office of Scientific Research under Award No. FA9559-21-1-0423.

- 
- [1] L. Šmejkal, J. Sinova, and T. Jungwirth, *Physical Review X* **12**, 031042 (2022).
  - [2] L. Šmejkal, R. González-Hernández, T. Jungwirth, and J. Sinova, *Science advances* **6**, eaaz8809 (2020), arXiv:1901.00445.
  - [3] L. Šmejkal, A. Marmodoro, K.-H. Ahn, R. González-Hernández, I. Turek, S. Mankovsky, H. Ebert, S. W. D'Souza, O. Šipr, J. Sinova, *et al.*, *Physical Review Letters* **131**, 256703 (2023).
  - [4] L. Šmejkal, J. Sinova, and T. Jungwirth, *Physical Review X* **12**, 040501 (2022).
  - [5] T. Jungwirth, R. Fernandes, E. Fradkin, A. MacDonald, J. Sinova, and L. Smejkal, arXiv preprint arXiv:2411.00717 (2024).
  - [6] J. Krempaský, L. Šmejkal, S. D'souza, M. Hajlaoui, G. Springholz, K. Uhlřřová, F. Alarab, P. Constantinou, V. Strocov, D. Usanov, *et al.*, *Nature* **626**, 517 (2024).
  - [7] S. Lee, S. Lee, S. Jung, J. Jung, D. Kim, Y. Lee, B. Seok, J. Kim, B. G. Park, L. Šmejkal, *et al.*, *Physical Review Letters* **132**, 036702 (2024).
  - [8] T. Osumi, S. Souma, T. Aoyama, K. Yamauchi, A. Honma, K. Nakayama, T. Takahashi, K. Ohgushi, and T. Sato, *Physical Review B* **109**, 115102 (2024).
  - [9] S. Reimers, L. Odenbreit, L. Šmejkal, V. N. Strocov, P. Constantinou, A. B. Hellenes, R. Jaeschke Ubierno, W. H. Campos, V. K. Bharadwaj, A. Chakraborty, *et al.*, *Nature Communications* **15**, 2116 (2024).
  - [10] G. Yang, Z. Li, S. Yang, J. Li, H. Zheng, W. Zhu, S. Cao, W. Zhao, J. Zhang, M. Ye, *et al.*, arXiv preprint arXiv:2405.12575 (2024).
  - [11] J. Ding, Z. Jiang, X. Chen, Z. Tao, Z. Liu, J. Liu, T. Li, J. Liu, Y. Yang, R. Zhang, *et al.*, arXiv preprint arXiv:2405.12687 (2024).
  - [12] M. Zeng, M.-Y. Zhu, Y.-P. Zhu, X.-R. Liu, X.-M. Ma, Y.-J. Hao, P. Liu, G. Qu, Y. Yang, Z. Jiang, *et al.*, *Advanced Science*, 2406529 (2024).
  - [13] C. Li, M. Hu, Z. Li, Y. Wang, W. Chen, B. Thiagarajan, M. Leandersson, C. Polley, T. Kim, H. Liu, *et al.*, arXiv preprint arXiv:2405.14777 (2024).
  - [14] A. Hariki, A. Dal Din, O. Amin, T. Yamaguchi, A. Badura, D. Kriegner, K. Edmonds, R. Champion, P. Wadley, D. Backes, *et al.*, *Physical Review Letters*

- 132**, 176701 (2024).
- [15] O. Amin, A. Dal Din, E. Golias, Y. Niu, A. Zakharov, S. Fromage, C. Fields, S. Heywood, R. Cousins, F. Maccherozzi, *et al.*, *Nature* **636**, 348 (2024).
- [16] I. I. Mazin, K. Koepf, M. D. Johannes, R. González-Hernández, and L. Šmejkal, *Proceedings of the National Academy of Sciences* **118**, e2108924118 (2021), arXiv:2105.06356.
- [17] K.-H. Ahn, A. Hariki, K.-W. Lee, and J. Kuneš, *Physical Review B* **99**, 184432 (2019), arXiv:1902.04436.
- [18] M. Naka, S. Hayami, H. Kusunose, Y. Yanagi, Y. Motome, and H. Seo, *Nature communications* **10**, 4305 (2019), arXiv:1902.02506.
- [19] R. González-Hernández, L. Šmejkal, K. Vyborný, Y. Yahagi, J. Sinova, T. Jungwirth, and J. Zelezny, *Physical Review Letters* **126**, 127701 (2021), arXiv:2002.07073.
- [20] L. Šmejkal, A. B. Hellenes, R. González-Hernández, J. Sinova, and T. Jungwirth, *Physical Review X* **12**, 011028 (2022), arXiv:2103.12664.
- [21] K. Samanta, M. Ležaić, M. Merte, F. Freimuth, S. Blügel, and Y. Mokrousov, *Journal of applied physics* **127** (2020), arXiv:2002.05393.
- [22] Z. Feng, X. Zhou, L. Šmejkal, L. Wu, Z. Zhu, H. Guo, R. González-Hernández, X. Wang, H. Yan, P. Qin, *et al.*, *Nature Electronics* **5**, 735 (2022).
- [23] H. Reichlova, R. Lopes Seeger, R. González-Hernández, I. Kounta, R. Schlitz, D. Kriegner, P. Ritzinger, M. Lammel, M. Leiviskä, A. Birk Hellenes, *et al.*, *Nature Communications* **15**, 4961 (2024).
- [24] L. Bai, W. Feng, S. Liu, L. Šmejkal, Y. Mokrousov, and Y. Yao, *Advanced Functional Materials*, 2409327 (2024).
- [25] D.-F. Shao, S.-H. Zhang, M. Li, C.-B. Eom, and E. Y. Tsybal, *Nature Communications* **12**, 7061 (2021), arXiv:2103.09219.
- [26] Y. Guo, H. Liu, O. Janson, I. C. Fulga, J. van den Brink, and J. I. Facio, *Materials Today Physics* **32**, 100991 (2023).
- [27] V. Leeb, A. Mook, L. Šmejkal, and J. Knolle, *Physical Review Letters* **132**, 236701 (2024).
- [28] M. Dürrnagel, H. Hohmann, A. Maity, J. Seufert, M. Klett, L. Klebl, and R. Thomale, arXiv preprint arXiv:2412.14251 (2024).
- [29] S. Bhowal and N. A. Spaldin, *Physical Review X* **14**, 011019 (2024).
- [30] R. M. Fernandes, V. S. De Carvalho, T. Birol, and R. G. Pereira, *Physical Review B* **109**, 024404 (2024).
- [31] X. Verbeek, D. Voderholzer, S. Schären, Y. Gachnang, N. Spaldin, and S. Bhowal, *Physical Review Research* **6**, 043157 (2024).
- [32] D. D. Maharaj, G. Sala, M. B. Stone, E. Kermarrec, C. Ritter, F. Fauth, C. A. Marjerrison, J. E. Greedan, A. Paramekanti, and B. D. Gaulin, *Physical Review Letters* **124**, 87206 (2020), arXiv:1909.03113.
- [33] A. Paramekanti, D. D. Maharaj, and B. D. Gaulin, *Physical Review B* **101**, 054439 (2020).
- [34] S. Voleti, A. Haldar, and A. Paramekanti, *Physical Review B* **104**, 174431 (2021).
- [35] A. Bose, N. J. Schreiber, R. Jain, D.-F. Shao, H. P. Nair, J. Sun, X. S. Zhang, D. A. Muller, E. Y. Tsybal, D. G. Schlom, *et al.*, *Nature Electronics* **5**, 267 (2022).
- [36] M. A. Blanco, M. Flórez, and M. Bermejo, *Journal of Molecular Structure: THEOCHEM* **419**, 19 (1997).
- [37] P. Santini and G. Amoretti, *Physical Review Letters* **85**, 2188 (2000).
- [38] L. Zhao, D. Torchinsky, H. Chu, V. Ivanov, R. Lifshitz, R. Flint, T. Qi, G. Cao, and D. Hsieh, *Nature Physics* **12**, 32 (2016).
- [39] C.-C. Wei, X. Li, S. Hatt, X. Huai, J. Liu, B. Singh, K.-M. Kim, R. M. Fernandes, P. Cardon, L. Zhao, *et al.*, arXiv preprint arXiv:2410.14542 (2024).
- [40] S. Landsgesell, E. Blumenroether, and K. Prokeš, *Journal of Physics: Condensed Matter* **25**, 086004 (2013).
- [41] D. G. Free, N. D. Withers, P. J. Hickey, and J. S. Evans, *Chemistry of Materials* **23**, 1625 (2011).
- [42] E. H. Lieb, *Physical review letters* **62**, 1201 (1989).
- [43] M. Inui, S. A. Trugman, and E. Abrahams, *Physical Review B* **49**, 3190 (1994).
- [44] C. Thompson, J. Carlo, R. Flacau, T. Aharen, I. Leahy, J. Pollicemi, T. Munsie, T. Medina, G. Luke, J. Munevar, *et al.*, *Journal of Physics: Condensed Matter* **26**, 306003 (2014).
- [45] D. Fiore Mosca, L. V. Pourovskii, and C. Franchini, *Physical Review B* **106**, 035127 (2022).
- [46] J. P. Allen and G. W. Watson, *Physical Chemistry Chemical Physics* **16**, 21016 (2014).
- [47] A. Liechtenstein, V. I. Anisimov, and J. Zaanen, *Physical Review B* **52**, R5467 (1995).
- [48] P. Lemoine, A. Verniere, M. Pasturel, G. Venturini, and B. Malaman, *Inorganic Chemistry* **57**, 2546 (2018).
- [49] B. Jiang, M. Hu, J. Bai, Z. Song, C. Mu, G. Qu, W. Li, W. Zhu, H. Pi, Z. Wei, *et al.*, arXiv preprint arXiv:2408.00320.
- [50] F. Zhang, X. Cheng, Z. Yin, C. Liu, L. Deng, Y. Qiao, Z. Shi, S. Zhang, J. Lin, Z. Liu, *et al.*, arXiv preprint arXiv:2407.19555 (2024).
- [51] M.-T. Suzuki, T. Koretsune, M. Ochi, and R. Arita, *Physical Review B* **95**, 094406 (2017), arXiv:1611.06042.
- [52] A. B. Hellenes, T. Jungwirth, J. Sinova, and L. Šmejkal, arXiv preprint arXiv:2309.01607 (2023).
- [53] S. Lovesey, E. Balcar, C. Detlefs, G. Van der Laan, D. Sivia, and U. Staub, *Journal of Physics: Condensed Matter* **15**, 4511 (2003).
- [54] Y. Aoki, S. Sanada, D. Kikuchi, H. Sugawara, and H. Sato, *Physica B: Condensed Matter* **403**, 1574 (2008).
- [55] T. Matsumura, T. Yonemura, K. Kunimori, M. Sera, and F. Iga, *Physical review letters* **103**, 017203 (2009).
- [56] R. Sibille, N. Gauthier, E. Lhotel, V. Porée, V. Pomjakushin, R. A. Ewings, T. G. Perring, J. Ollivier, A. Wildes, C. Ritter, *et al.*, *Nature physics* **16**, 546 (2020).
- [57] M. Tsujimoto, Y. Matsumoto, T. Tomita, A. Sakai, and S. Nakatsuji, *Physical review letters* **113**, 267001 (2014).
- [58] F. Freyer, J. Attig, S. Lee, A. Paramekanti, S. Trebst, and Y. B. Kim, *Physical Review B* **97**, 115111 (2018).
- [59] A. S. Patri, A. Sakai, S. Lee, A. Paramekanti, S. Nakatsuji, and Y. B. Kim, *Nature Communications* **10**, 4092 (2019).
- [60] M. E. Sorensen and I. R. Fisher, *Physical Review B* **103**, 155106 (2021).
- [61] L. Ye, M. E. Sorensen, M. D. Bachmann, and I. R. Fisher, *Nature Communications* **15**, 7005 (2024).